Inclusive cross section and double helicity asymmetry for π^0 production in $p+p$ collisions at $\sqrt{s} = 62.4$ GeV

A. Adare,[12] S. Afanasiev,[26] C. Aidala,[37] N.N. Ajitanand,[54] Y. Akiba,[48, 49] H. Al-Bataineh,[43] J. Alexander,[54]
K. Aoki,[31, 48] L. Aphecetche,[56] J. Asai,[48] E.T. Atomssa,[32] R. Averbeck,[55] T.C. Awes,[44] B. Azmoun,[7]
V. Babintsev,[22] M. Bai,[6] G. Baksay,[18] L. Baksay,[18] A. Baldisseri,[15] K.N. Barish,[8] P.D. Barnes,[34] B. Bassalleck,[42]
A.T. Basye,[1] S. Bathe,[8] S. Batsouli,[44] V. Baublis,[47] C. Baumann,[38] A. Bazilevsky,[7] S. Belikov,[7, *] R. Bennett,[55]
A. Berdnikov,[51] Y. Berdnikov,[51] A.A. Bickley,[12] J.G. Boissevain,[34] H. Borel,[15] K. Boyle,[55] M.L. Brooks,[34]
H. Buesching,[7] V. Bumazhnov,[22] G. Bunce,[7, 49] S. Butsyk,[34] C.M. Camacho,[34] S. Campbell,[55] P. Chand,[4]
B.S. Chang,[63] W.C. Chang,[2] J.-L. Charvet,[15] S. Chernichenko,[22] C.Y. Chi,[13] M. Chiu,[23] I.J. Choi,[63]
R.K. Choudhury,[4] T. Chujo,[59] P. Chung,[54] A. Churyn,[22] V. Cianciolo,[44] B.A. Cole,[13] P. Constantin,[34] M. Csanád,[17]
T. Csörgő,[28] T. Dahms,[55] S. Dairaku,[31, 48] K. Das,[19] G. David,[7] A. Denisov,[22] D. d'Enterria,[32] A. Deshpande,[49, 55]
E.J. Desmond,[7] O. Dietzsch,[52] A. Dion,[55] M. Donadelli,[52] O. Drapier,[32] A. Drees,[55] K.A. Drees,[6] A.K. Dubey,[62]
A. Durum,[22] D. Dutta,[4] V. Dzhordzhadze,[8] Y.V. Efremenko,[44] J. Egdemir,[55] F. Ellinghaus,[12] T. Engelmore,[13]
A. Enokizono,[33] H. En'yo,[48, 49] S. Esumi,[59] K.O. Eyser,[8] B. Fadem,[39] D.E. Fields,[42, 49] M. Finger,[9] M. Finger, Jr.,[9]
F. Fleuret,[32] S.L. Fokin,[30] Z. Fraenkel,[62, *] J.E. Frantz,[55] A. Franz,[7] A.D. Frawley,[19] K. Fujiwara,[48]
Y. Fukao,[31, 48] T. Fusayasu,[41] I. Garishvili,[57] A. Glenn,[12] H. Gong,[55] M. Gonin,[32] J. Gosset,[15] Y. Goto,[48, 49]
R. Granier de Cassagnac,[32] N. Grau,[13] S.V. Greene,[60] M. Grosse Perdekamp,[23, 49] T. Gunji,[11] H.-Å. Gustafsson,[36]
A. Hadj Henni,[56] J.S. Haggerty,[7] H. Hamagaki,[11] R. Han,[46] E.P. Hartouni,[33] K. Haruna,[21] E. Haslum,[36]
R. Hayano,[11] M. Heffner,[33] T.K. Hemmick,[55] T. Hester,[8] X. He,[20] J.C. Hill,[25] M. Hohlmann,[18] W. Holzmann,[54]
K. Homma,[21] B. Hong,[29] T. Horaguchi,[11, 48, 58] D. Hornback,[57] S. Huang,[60] T. Ichihara,[48, 49] R. Ichimiya,[48]
Y. Ikeda,[59] K. Imai,[31, 48] J. Imrek,[16] M. Inaba,[59] D. Isenhower,[1] M. Ishihara,[48] T. Isobe,[11] M. Issah,[54] A. Isupov,[26]
D. Ivanischev,[47] B.V. Jacak,[55, †] J. Jia,[13] J. Jin,[13] B.M. Johnson,[7] K.S. Joo,[40] D. Jouan,[45] F. Kajihara,[11]
S. Kametani,[48] N. Kamihara,[49] J. Kamin,[55] J.H. Kang,[63] J. Kapustinsky,[34] D. Kawall,[37, 49] A.V. Kazantsev,[30]
T. Kempel,[25] A. Khanzadeev,[47] K. Kijima,[21] J. Kikuchi,[61] B.I. Kim,[29] D.H. Kim,[40] D.J. Kim,[63] E. Kim,[53]
S.H. Kim,[63] E. Kinney,[12] K. Kiriluk,[12] A. Kiss,[17] E. Kistenev,[7] J. Klay,[33] C. Klein-Boesing,[38] L. Kochenda,[47]
V. Kochetkov,[22] B. Komkov,[47] M. Konno,[59] J. Koster,[23] A. Kozlov,[62] A. Král,[14] A. Kravitz,[13] G.J. Kunde,[34]
K. Kurita,[50, 48] M. Kurosawa,[48] M.J. Kweon,[29] Y. Kwon,[57] G.S. Kyle,[43] R. Lacey,[54] Y.S. Lai,[13] J.G. Lajoie,[25]
D. Layton,[23] A. Lebedev,[25] D.M. Lee,[34] K.B. Lee,[29] T. Lee,[53] M.J. Leitch,[34] M.A.L. Leite,[52] B. Lenzi,[52]
P. Liebing,[49] T. Liška,[14] A. Litvinenko,[26] H. Liu,[43] M.X. Liu,[34] X. Li,[10] B. Love,[60] D. Lynch,[7] C.F. Maguire,[60]
Y.I. Makdisi,[6] A. Malakhov,[26] M.D. Malik,[42] V.I. Manko,[30] E. Mannel,[13] Y. Mao,[46, 48] L. Mašek,[9, 24] H. Masui,[59]
F. Matathias,[13] M. McCumber,[55] P.L. McGaughey,[34] B. Meredith,[23] Y. Miake,[59] P. Mikeš,[24] K. Miki,[59] A. Milov,[7]
M. Mishra,[3] J.T. Mitchell,[7] A.K. Mohanty,[4] Y. Morino,[11] A. Morreale,[8] D.P. Morrison,[7] T.V. Moukhanova,[30]
D. Mukhopadhyay,[60] J. Murata,[50, 48] S. Nagamiya,[27] J.L. Nagle,[12] M. Naglis,[62] M. Nagy,[17] I. Nakagawa,[48, 49]
Y. Nakamiya,[21] T. Nakamura,[21] K. Nakano,[48, 58] J. Newby,[33] M. Nguyen,[55] T. Niita,[59] R. Nouicer,[5]
A.S. Nyanin,[30] E. O'Brien,[7] S.X. Oda,[11] C.A. Ogilvie,[25] H. Okada,[31, 48] K. Okada,[49] M. Oka,[59] Y. Onuki,[48]
A. Oskarsson,[36] M. Ouchida,[21] K. Ozawa,[11] R. Pak,[5] A.P.T. Palounek,[34] V. Pantuev,[55] V. Papavassiliou,[43]
J. Park,[53] W.J. Park,[29] S.F. Pate,[43] H. Pei,[25] J.-C. Peng,[23] H. Pereira,[15] V. Peresedov,[26] D.Yu. Peressounko,[30]
C. Pinkenburg,[7] M.L. Purschke,[7] A.K. Purwar,[34] H. Qu,[20] J. Rak,[42] A. Rakotozafindrabe,[32] I. Ravinovich,[62]
K.F. Read,[44, 57] S. Rembeczki,[18] M. Reuter,[55] K. Reygers,[38] V. Riabov,[47] Y. Riabov,[47] D. Roach,[60] G. Roche,[35]
S.D. Rolnick,[8] M. Rosati,[25] S.S.E. Rosendahl,[36] P. Rosnet,[35] P. Rukoyatkin,[26] P. Ružička,[24] V.L. Rykov,[48]
B. Sahlmueller,[38] N. Saito,[31, 48, 49] T. Sakaguchi,[7] S. Sakai,[59] K. Sakashita,[48, 58] V. Samsonov,[47] T. Sato,[59]
S. Sawada,[27] K. Sedgwick,[8] J. Seele,[12] R. Seidl,[23] A.Yu. Semenov,[25] V. Semenov,[22] R. Seto,[8] D. Sharma,[62]
I. Shein,[22] T.-A. Shibata,[48, 58] K. Shigaki,[21] M. Shimomura,[59] K. Shoji,[31, 48] P. Shukla,[4] A. Sickles,[7] C.L. Silva,[52]
D. Silvermyr,[44] C. Silvestre,[15] K.S. Sim,[29] B.K. Singh,[3] C.P. Singh,[3] V. Singh,[3] M. Slunečka,[9] A. Soldatov,[22]
R.A. Soltz,[33] W.E. Sondheim,[34] S.P. Sorensen,[57] I.V. Sourikova,[7] F. Staley,[15] P.W. Stankus,[44] E. Stenlund,[36]
M. Stepanov,[43] A. Ster,[28] S.P. Stoll,[7] T. Sugitate,[21] C. Suire,[45] A. Sukhanov,[5] J. Sziklai,[28] E.M. Takagui,[52]
A. Taketani,[48, 49] R. Tanabe,[59] Y. Tanaka,[41] K. Tanida,[48, 49] M.J. Tannenbaum,[7] A. Taranenko,[54] P. Tarján,[16]
T.L. Thomas,[42] M. Togawa,[31, 48] A. Toia,[55] L. Tomášek,[24] Y. Tomita,[59] H. Torii,[48] R.S. Towell,[1] V-N. Tram,[32]
I. Tserruya,[62] Y. Tsuchimoto,[21] C. Vale,[25] H. Valle,[60] H.W. van Hecke,[34] A. Veicht,[23] J. Velkovska,[60] R. Vertesi,[16]
A.A. Vinogradov,[30] M. Virius,[14] V. Vrba,[24] E. Vznuzdaev,[47] D. Walker,[55] X.R. Wang,[43] Y. Watanabe,[48, 49]
F. Wei,[25] J. Wessels,[38] S.N. White,[7] S. Williamson,[23] D. Winter,[13] C.L. Woody,[7] M. Wysocki,[12] W. Xie,[49]
Y.L. Yamaguchi,[61] K. Yamaura,[21] R. Yang,[23] A. Yanovich,[22] J. Ying,[20] S. Yokkaichi,[48, 49] G.R. Young,[44]

I. Younus,[42] I.E. Yushmanov,[30] W.A. Zajc,[13] O. Zaudtke,[38] C. Zhang,[44] S. Zhou,[10] and L. Zolin[26]
(PHENIX Collaboration)
[1]*Abilene Christian University, Abilene, TX 79699, U.S.*
[2]*Institute of Physics, Academia Sinica, Taipei 11529, Taiwan*
[3]*Department of Physics, Banaras Hindu University, Varanasi 221005, India*
[4]*Bhabha Atomic Research Centre, Bombay 400 085, India*
[5]*Chemistry Department, Brookhaven National Laboratory, Upton, NY 11973-5000, U.S.*
[6]*Collider-Accelerator Department, Brookhaven National Laboratory, Upton, NY 11973-5000, U.S.*
[7]*Physics Department, Brookhaven National Laboratory, Upton, NY 11973-5000, U.S.*
[8]*University of California - Riverside, Riverside, CA 92521, U.S.*
[9]*Charles University, Ovocný trh 5, Praha 1, 116 36, Prague, Czech Republic*
[10]*China Institute of Atomic Energy (CIAE), Beijing, People's Republic of China*
[11]*Center for Nuclear Study, Graduate School of Science, University of Tokyo, 7-3-1 Hongo, Bunkyo, Tokyo 113-0033, Japan*
[12]*University of Colorado, Boulder, CO 80309, U.S.*
[13]*Columbia University, New York, NY 10027 and Nevis Laboratories, Irvington, NY 10533, U.S.*
[14]*Czech Technical University, Zikova 4, 166 36 Prague 6, Czech Republic*
[15]*Dapnia, CEA Saclay, F-91191, Gif-sur-Yvette, France*
[16]*Debrecen University, H-4010 Debrecen, Egyetem tér 1, Hungary*
[17]*ELTE, Eötvös Loránd University, H - 1117 Budapest, Pázmány P. s. 1/A, Hungary*
[18]*Florida Institute of Technology, Melbourne, FL 32901, U.S.*
[19]*Florida State University, Tallahassee, FL 32306, U.S.*
[20]*Georgia State University, Atlanta, GA 30303, U.S.*
[21]*Hiroshima University, Kagamiyama, Higashi-Hiroshima 739-8526, Japan*
[22]*IHEP Protvino, State Research Center of Russian Federation, Institute for High Energy Physics, Protvino, 142281, Russia*
[23]*University of Illinois at Urbana-Champaign, Urbana, IL 61801, U.S.*
[24]*Institute of Physics, Academy of Sciences of the Czech Republic, Na Slovance 2, 182 21 Prague 8, Czech Republic*
[25]*Iowa State University, Ames, IA 50011, U.S.*
[26]*Joint Institute for Nuclear Research, 141980 Dubna, Moscow Region, Russia*
[27]*KEK, High Energy Accelerator Research Organization, Tsukuba, Ibaraki 305-0801, Japan*
[28]*KFKI Research Institute for Particle and Nuclear Physics of the Hungarian Academy of Sciences (MTA KFKI RMKI), H-1525 Budapest 114, POBox 49, Budapest, Hungary*
[29]*Korea University, Seoul, 136-701, Korea*
[30]*Russian Research Center "Kurchatov Institute", Moscow, Russia*
[31]*Kyoto University, Kyoto 606-8502, Japan*
[32]*Laboratoire Leprince-Ringuet, Ecole Polytechnique, CNRS-IN2P3, Route de Saclay, F-91128, Palaiseau, France*
[33]*Lawrence Livermore National Laboratory, Livermore, CA 94550, U.S.*
[34]*Los Alamos National Laboratory, Los Alamos, NM 87545, U.S.*
[35]*LPC, Université Blaise Pascal, CNRS-IN2P3, Clermont-Fd, 63177 Aubiere Cedex, France*
[36]*Department of Physics, Lund University, Box 118, SE-221 00 Lund, Sweden*
[37]*Department of Physics, University of Massachusetts, Amherst, MA 01003-9337, U.S.*
[38]*Institut für Kernphysik, University of Muenster, D-48149 Muenster, Germany*
[39]*Muhlenberg University, Allentown, PA 18104-5586, U.S.*
[40]*Myongji University, Yongin, Kyonggido 449-728, Korea*
[41]*Nagasaki Institute of Applied Science, Nagasaki-shi, Nagasaki 851-0193, Japan*
[42]*University of New Mexico, Albuquerque, NM 87131, U.S.*
[43]*New Mexico State University, Las Cruces, NM 88003, U.S.*
[44]*Oak Ridge National Laboratory, Oak Ridge, TN 37831, U.S.*
[45]*IPN-Orsay, Universite Paris Sud, CNRS-IN2P3, BP1, F-91406, Orsay, France*
[46]*Peking University, Beijing, People's Republic of China*
[47]*PNPI, Petersburg Nuclear Physics Institute, Gatchina, Leningrad region, 188300, Russia*
[48]*RIKEN, The Institute of Physical and Chemical Research, Wako, Saitama 351-0198, Japan*
[49]*RIKEN BNL Research Center, Brookhaven National Laboratory, Upton, NY 11973-5000, U.S.*
[50]*Physics Department, Rikkyo University, 3-34-1 Nishi-Ikebukuro, Toshima, Tokyo 171-8501, Japan*
[51]*Saint Petersburg State Polytechnic University, St. Petersburg, Russia*
[52]*Universidade de São Paulo, Instituto de Física, Caixa Postal 66318, São Paulo CEP05315-970, Brazil*
[53]*System Electronics Laboratory, Seoul National University, Seoul, Korea*
[54]*Chemistry Department, Stony Brook University, Stony Brook, SUNY, NY 11794-3400, U.S.*
[55]*Department of Physics and Astronomy, Stony Brook University, SUNY, Stony Brook, NY 11794, U.S.*
[56]*SUBATECH (Ecole des Mines de Nantes, CNRS-IN2P3, Université de Nantes) BP 20722 - 44307, Nantes, France*
[57]*University of Tennessee, Knoxville, TN 37996, U.S.*
[58]*Department of Physics, Tokyo Institute of Technology, Oh-okayama, Meguro, Tokyo 152-8551, Japan*
[59]*Institute of Physics, University of Tsukuba, Tsukuba, Ibaraki 305, Japan*
[60]*Vanderbilt University, Nashville, TN 37235, U.S.*

[61] *Waseda University, Advanced Research Institute for Science and Engineering, 17 Kikui-cho, Shinjuku-ku, Tokyo 162-0044, Japan*
[62] *Weizmann Institute, Rehovot 76100, Israel*
[63] *Yonsei University, IPAP, Seoul 120-749, Korea*

(Dated: October 3, 2008)

The PHENIX experiment presents results from the RHIC 2006 run with polarized $p+p$ collisions at $\sqrt{s} = 62.4$ GeV, for inclusive π^0 production at mid-rapidity. Unpolarized cross section results are measured for transverse momenta $p_T = 0.5$ to 7 GeV/c. Next-to-leading order perturbative quantum chromodynamics calculations are compared with the data, and while the calculations are consistent with the measurements, next-to-leading logarithmic corrections improve the agreement. Double helicity asymmetries A_{LL} are presented for $p_T = 1$ to 4 GeV/c and probe the higher range of Bjorken x of the gluon (x_g) with better statistical precision than our previous measurements at $\sqrt{s} = 200$ GeV. These measurements are sensitive to the gluon polarization in the proton for $0.06 < x_g < 0.4$.

PACS numbers: 13.85.Ni,13.88.+e,21.10.Hw,25.40.Ep

I. INTRODUCTION

Spin is a property of particles as fundamental as charge and mass. The spin of the proton was first determined in the 1920s, yet we still do not have a detailed understanding of what inside the proton makes up the spin of the proton. Polarized lepton-nucleon deep-inelastic scattering (DIS) experiments have revealed that only ∼25% of the proton spin can be attributed to the spins of the quarks and anti-quarks [1, 2] indicating that the proton spin must be largely carried by the spin of the gluons and/or orbital angular momentum of quarks and gluons. Polarized proton-proton collisions at the Relativistic Heavy-Ion Collider (RHIC) provide a laboratory to study the gluon-spin contribution to the proton spin structure, ΔG, with strongly interacting probes via measurements of double helicity asymmetries (A_{LL}) [3].

The A_{LL} of π^0's is defined as

$$A_{LL}^{\pi^0} = \frac{\sigma_{++} - \sigma_{+-}}{\sigma_{++} + \sigma_{+-}}, \tag{1}$$

where $\sigma_{++}(\sigma_{+-})$ represents the π^0 production cross section in polarized $p+p$ collisions with the same (opposite) helicities. In leading order (LO) perturbative Quantum Chromodynamics (pQCD), π^0 production is the sum of all possible subprocesses $ab \rightarrow cX$, where a,b represent the initial partons in the protons, c is the final state parton which fragments into a π^0, and X is the unobserved parton. Then A_{LL} is calculated as

$$A_{LL}^{\pi^0} = \frac{\Sigma_{a,b,c}\Delta f_a \Delta f_b \hat{\sigma}^{[ab\rightarrow cX]}\hat{a}_{LL}^{[ab\rightarrow cX]}D_c^{\pi^0}}{\Sigma_{a,b,c} f_a f_b \hat{\sigma}^{[ab\rightarrow cX]}D_c^{\pi^0}}, \tag{2}$$

where $f_{a,b}$ represent unpolarized parton distribution functions (PDF) of parton a, b and $\Delta f_{a,b}$ represent polarized PDFs, $D_c^{\pi^0}$ is a fragmentation function (FF) of parton c to π^0, $\hat{\sigma}^{[ab\rightarrow cX]}$ and $\hat{a}_{LL}^{[ab\rightarrow cX]}$ denote respectively the cross section and A_{LL} of the subprocess $ab \rightarrow cX$. The sum is performed for all possible partons (quarks and gluons). The Bjorken-x dependence of the PDFs, the kinematical dependence of the FFs, and the integral over all possible kinematics are omitted in the equation. The partonic quantities $\hat{\sigma}$ and $\hat{a}_{LL}$ can be calculated in pQCD. Since π^0 production is dominated by gluon-gluon and quark-gluon scattering in the measured p_T range ($p_T < 4$ GeV/c), A_{LL} is directly sensitive to the polarized gluon distribution function in the proton.

Cross section measurements at RHIC have established the validity of using a next-to-leading order (NLO) pQCD description at $\sqrt{s} = 200$ GeV for inclusive mid-rapidity π^0 [4, 5] and forward π^0 production [6], and for mid-rapidity jet [7] and direct photon production [8]. However, at lower center of mass energy, NLO pQCD calculations have been less successful in describing the data [9]. The inclusion of "threshold resummation" at next-to-leading logarithmic accuracy (NLL) [10] improves the agreement between theory and data at fixed-target energies. While taking into account threshold logarithms at the fixed-target kinematic region is essential, they may also need to be accounted for at $\sqrt{s} = 62.4$ GeV, but will provide a smaller effect [11].

A precise measurement of the inclusive π^0 production cross section at $\sqrt{s} = 62.4$ GeV is important for the heavy-ion program at RHIC. A new state of dense matter is formed in Au+Au collisions at 200 GeV and parton energy loss in the produced dense medium results in high p_T leading hadron suppression. Measurements of high p_T data at lower energies are of great importance in identifying the energy range at which the suppression sets in. However, they require solid measurements of the cross section in $p+p$ collisions as a baseline for medium effects. At the ISR, inclusive neutral and charged pion cross sections were measured several times at $\sqrt{s} \sim 62$ GeV [12, 13], but they have large uncertainties and have a large variation [14]. Having both heavy-ion and baseline $p+p$ measurements with the same experiment is advantageous as it leads to a reduction of

---

[*] Deceased

[†] PHENIX Spokesperson: jacak@skipper.physics.sunysb.edu

the systematic uncertainties and, thus, to a more precise relative comparison of the data.

In this paper, we present results on inclusive neutral pion production at mid-rapidity from proton-proton collisions at $\sqrt{s} = 62.4$ GeV from data collected during the RHIC 2006 run. A sample of events from longitudinally polarized $p + p$ collisions (about 2/3 of the total data sample) was used for double helicity asymmetry measurements. The other events from the 2006 data sample were from transversely polarized $p + p$ collisions and, along with the longitudinally polarized data, were used for the unpolarized cross section measurements, by averaging over the different initial spin states.

The structure of this paper is as follows. The PHENIX subsystems used in this analysis are briefly introduced in section II. The unpolarized π^0 cross section analysis and the results are discussed in section III. The π^0 A_{LL} analysis and the results follow in section IV, and a summary is given in section V.

II. EXPERIMENT

The PHENIX experiment at RHIC measured π^0's via $\pi^0 \rightarrow \gamma\gamma$ decays using a highly segmented ($\Delta\eta \times \Delta\phi \sim 0.01 \times 0.01$) electromagnetic calorimeter (EMCal) [15], covering a pseudorapidity range of $|\eta| < 0.35$ and azimuthal angle range of $\Delta\phi = \pi$. The EMCal comprises two calorimeter types: 6 sectors of lead scintillator sampling calorimeter (PbSc) and 2 sectors of a lead glass Cherenkov calorimeter (PbGl). Each of the EMCal towers was calibrated by the two-photon invariant mass from π^0 decays and cross checked against the energy deposited by the minimum ionizing particles in the EMCal, and the correlation between the measured momenta of electron and positron tracks and the associated energy deposited in the EMCal. The uncertainty on the absolute energy scale was 1.2%.

The π^0 data in this analysis were collected using two different triggers. One is a beam-beam counter (BBC) trigger which was defined by the coincidence of signals in two BBCs located at pseudorapidities $\pm(3.0 - 3.9)$ with full azimuthal coverage [16]. The time difference between the two BBCs was used to determine the collision vertex along the beam axis, which in this analysis was required to be within 30 cm from the center of the PHENIX interaction region (IR). The other trigger is an EMCal-based high p_T photon trigger, in which threshold discrimination corresponding to a deposited energy of 0.8 GeV was applied independently to sums of analog signals from 2×2 groupings of adjacent EMCal towers [4]. This trigger had limited efficiency for π^0 detection at low p_T (e.g. 50% in 1.0–1.5 GeV/c p_T bin) and close to 100% efficiency at $p_T >3$ GeV/c.

Beam-beam counters along with zero degree calorimeters (ZDC) [17], which detect neutral particles near the beam axis ($\theta < 2.5$ mrad), were utilized to determine the integrated luminosity for the analyzed data sample needed for the absolute normalization of the measured cross sections. Trigger counts defined with the BBCs and ZDCs were also used for the precise measurements of the relative luminosity between bunches with different spin configuration, and the spin dependence of very forward neutron production [5, 18, 19], detected by the ZDCs, served for monitoring the orientation of the beam polarization in the PHENIX interaction region (IR) through the run. These are necessary components of the spin asymmetry measurements.

III. THE $pp \rightarrow \pi^0 X$ CROSS SECTION

The unpolarized cross section analysis technique was very similar to our analyses of $\sqrt{s} = 200$ GeV data [4, 5] and is briefly discussed in section III A. Cross section measurements require an absolute determination of luminosity which is described in section III B. The π^0 cross section results are presented and discussed in section III C.

A. π^0 analysis

The π^0 yield in each p_T bin was determined from the two-photon invariant mass spectra. The background contribution under the π^0 peak in the two-photon invariant mass distribution varied from 75% in the lowest 0.5–0.75 GeV/c p_T bin to less than 4% for $p_T > 3$ GeV/c.

One of the main corrections applied to the measured π^0 spectrum is the BBC trigger bias f_{π^0}, which is defined as the fraction of high p_T π^0 events in the mid-rapidity spectrometer acceptance which fire the BBC trigger. This fraction was determined from the ratio of the number of reconstructed π^0 in the high p_T photon triggered sample with and without the BBC trigger requirement. As shown in Fig. 1, f_{π^0} was about 40% up to $p_T \sim 3$ GeV/c and then monotonically dropped down to 25% at $p_T \sim 7$ GeV/c. The drop can be explained by the fact that most of the energy is used for the production of high energy jets which contain the measured high p_T π^0 and there is not enough energy left to produce particles in the BBC acceptance $3.0 \leq |\eta| \leq 3.9$, which was optimized for $\sqrt{s} = 200$ GeV (where such a drop was not observed [4]) and was not moved for the present $\sqrt{s} = 62.4$ GeV measurements.

The main contributors to the systematic uncertainties of the measured π^0 spectrum are given in Table I. The "Energy scale" uncertainty includes uncertainties due to EMCal energy absolute calibration and nonlinearity. The "Yield extraction" uncertainty comes from the background subtraction. The "Yield correction" uncertainty comes from the correction for the geometric acceptance, trigger efficiency, reconstruction efficiencies, detector response, and photon conversion. The normalization uncertainty is not included and is discussed in section III B.

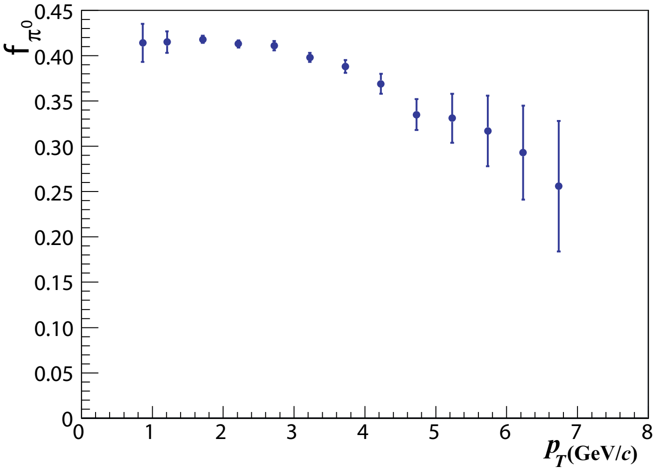

FIG. 1: (color online) The fraction of the inclusive π^0 yield which satisfied the BBC trigger condition.

TABLE I: Main systematic uncertainties in % of the π^0 spectrum from the PbSc for two representative p_T bins (the PbGl uncertainties are similar).

$\langle p_T \rangle$ (GeV/c)	1.2	6.7
Energy scale	3.9	13.1
Yield extraction	3.9	2.0
Yield correction	6.4	6.0

The data sets from the two EMCal subsystems, PbSc and PbGl, were analyzed separately and combined for the final results. Results from the two subsystems were consistent within uncertainties. The systematic uncertainty of the combined result is reduced as the major systematic uncertainties in the two EMCal subsystems are not correlated. For final π^0 cross section results, BBC-triggered events were used for $p_T < 3$ GeV/c and high p_T photon triggered events in coincidence with the BBC trigger were used for $p_T > 3$ GeV/c.

B. Vernier scan analysis

The measured π^0 cross section was normalized to the integrated luminosity for the analyzed data sample (L) which was determined from the number of BBC-triggered events using an absolute calibration of the BBC trigger cross section σ_{BBC}. The value of σ_{BBC} is obtained via the van der Meer or Vernier scan technique [20]. This is a crucial part of the absolute cross section analysis and is therefore discussed in detail in this section.

In a scan, the transverse widths of the beam overlap σ_x and σ_y were measured by sweeping one beam across the other in small steps while monitoring the BBC trigger rate. Then the instantaneous machine luminosity of each bunch crossing $L_{machine}$ is computed as:

$$L_{machine} = \frac{f_{rev}}{2\pi\sigma_x\sigma_y} \cdot N_B \cdot N_Y, \tag{3}$$

where N_B and N_Y are the bunch intensities of the two beams ($\sim 10^{11}$/bunch), f_{rev} is the revolution frequency (78 kHz). The BBC trigger cross section σ_{BBC} is the ratio of the BBC trigger rate when the beams were overlapping maximally (R_{max}) to the effective luminosity L_{eff}:

$$\sigma_{BBC} = R_{max}/L_{eff}, \tag{4}$$

where

$$L_{eff} = L_{machine} \cdot \epsilon_{\text{vertex}}, \tag{5}$$

and ϵ_{vertex} is the fraction of the number of collisions in the PHENIX interaction region (IR) within the BBC trigger vertex cut (usually $|z| < 30$ cm).

$L_{machine}$ was corrected for the z dependence of the transverse beam sizes caused by the beam focusing in the IR (hour-glass effect) and for the beam crossing angle. The value of ϵ_{vertex} was extracted from the z-vertex distribution of events measured by the BBCs and was corrected for the dependence of the BBC trigger efficiency on the collision vertex position z along the beam axis. These corrections are discussed in more detail below.

In $p+p$ collisions at $\sqrt{s} = 62.4$ GeV, the BBC trigger efficiency vs z shape was estimated from the comparison with a "detector unbiased" z-vertex distribution obtained from the convolution of colliding bunch intensity profiles along the z-axis as measured by Wall Current Monitors (WCMs) [21]. The correction factor of 0.83 ± 0.08 for ϵ_{vertex} in Eq. (5) was obtained, resulting in $\epsilon_{\text{vertex}} = 0.37 \pm 10\%$. This approach is confirmed in $p+p$ collisions at $\sqrt{s} = 200$ GeV where the ZDCs have enough efficiency to measure the z vertex distribution. The efficiency of the ZDCs (located at $z = \pm 18$ m) does not depend on collision vertex position in the PHENIX IR, which was distributed with a sigma of $0.5 - 0.7$ m around $z = 0$. The vertex distribution obtained with the WCMs is well reproduced by the measurement with the ZDCs at $\sqrt{s} = 200$ GeV (Fig. 2a).

Beam focusing in the IR causes bunch transverse sizes to vary away from the nominal collision point ($z = 0$) as $\sigma^2(z) = \sigma^2(z = 0) \times (1 + z^2/\beta^{*2})$, where β^* is the value of the betatron amplitude function at the interaction point. This is the so-called hour-glass effect. The product $\sigma_x\sigma_y$ in Eq. (3) should be replaced by an effective $\langle \sigma_x \cdot \sigma_y \rangle$, which differs from what was measured in a scan (mainly due to the vertex cut implemented in BBC trigger). The correction due to this effect for Vernier scan data at $\sqrt{s} = 62.4$ GeV with a betatron amplitude function at the collision point of $\beta^* = 3$ m was simulated with WCM data and calculated to be 0.93 ± 0.02. The applicability of our calculational technique is illustrated in Fig. 2 with the high statistics Vernier scan data at $\sqrt{s} = 200$ GeV.

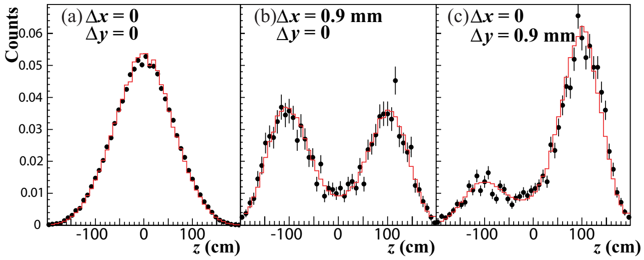

FIG. 2: (color online) Collision z-vertex distribution in the PHENIX IR measured by ZDCs in a Vernier scan at $\sqrt{s} = 200$ GeV (points) and calculations from convolution of colliding bunch intensity profiles along z-axis and including the hour-glass effect for $\beta^* = 1$ m, for bunches with typical length of 1 m and transverse size of 0.3 mm (histograms); (a) beams are head-on; (b) one beam is 0.9 mm displaced relative to the other beam in the horizontal direction (illustrates the hour-glass effect) and (c) one beam is 0.9 mm displaced relative to the other beam in the vertical direction. The calculations include the bunch crossing angle with a vertical projection of 0.15 mrad.

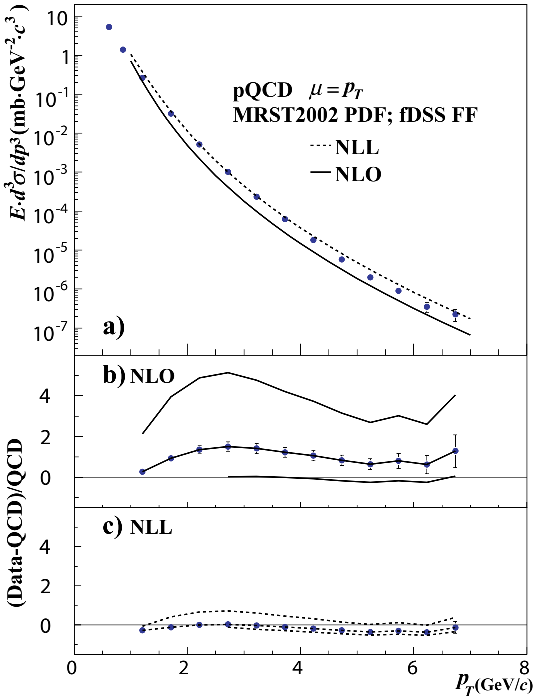

FIG. 3: (color online) (a) The neutral pion production cross section at $\sqrt{s} = 62.4$ GeV as a function of p_T (circles) and the results of NLO (solid) and NLL (dashed) pQCD calculations for the theory scale $\mu = p_T$. (b) The relative difference between the data and NLO pQCD calculations for the three theory scales $\mu = p_T/2$ (upper line), p_T (middle line) and $2p_T$ (lower line); experimental uncertainties (excluding the 11% normalization uncertainty) are shown for the $\mu = p_T$ curve. (c) The same as b) but for NLL pQCD calculations.

Figure 2b and 2c shows the sensitivity of our data for the transversely displaced beams to the hour-glass effect and to the crossing angle between the colliding beams, compared with a head-on vertex distribution in Fig. 2a. The two peaks in Fig. 2b and 2c, caused by the hour-glass effect, show an overlap of the diverging colliding beams at large $|z|$ in a particular displaced beam setting from a Vernier scan. The obvious asymmetry in the two peaks in Fig. 2c is a result of the non-zero crossing angle between colliding bunches. In all Vernier scan measurements the crossing angle was found to be less than 0.2 mrad, which translates to a negligible correction for $L_{machine}$ at $\sqrt{s} =$ 62.4 GeV, with a typical bunch length of $\sim$ 1 m and bunch transverse size of 1 mm.

After all the corrections discussed above were applied, our BBC trigger cross section in $p + p$ collisions at $\sqrt{s} = 62.4$ GeV was found to be $\sigma_{BBC} = 13.7$ mb with a systematic uncertainty of ± 1.5 mb ($\pm 11\%$), i.e. $\sim 40\%$ of the world-average value of the inelastic $p + p$ scattering cross section at $\sqrt{s} = 62.4$ GeV[14]. Major contributors to the systematic uncertainty are 4% from the uncertainty in the normalization of bunch intensity measurements and in the calibration of the beam position measurements in the Vernier scan, 10% from the BBC trigger efficiency correction of ϵ_{vertex}, and 2% from the hour-glass correction.

C. π^0 cross section results and discussion

Figure 3 presents the inclusive mid-rapidity π^0 invariant production cross section at $\sqrt{s} = 62.4$ GeV versus p_T, from $p_T = 0.5$ GeV/c to $p_T = 7$ GeV [23]. An overall normalization uncertainty of 11% due to the uncertainty in absolute normalization of the luminosity is not shown. The analyzed data sample with 0.76×10^9 BBC triggers corresponded to about 55 nb^{-1} integrated luminosity. The measurements fall within the large spread of ISR data [12, 13, 14].

The data are compared to NLO and NLL pQCD calculations at a theory scale $\mu = p_T$, where μ represents equal factorization, renormalization, and fragmentation scales [11]. The NLL corrections extend the NLO calculations to include the resummation of extra "threshold" logarithmic terms which appear in the perturbative expansion at not very high energies because the initial partons have just enough energy to produce the high p_T parton that fragments into a final pion. The MRST2002 parton distribution functions [24] and the fDSS set of fragmentation functions [25], which are extracted in NLO, are used in both NLO and NLL calculations. We have previously seen that the data are well described by NLO pQCD with a scale of $\mu = p_T$ at $\sqrt{s} = 200$ GeV [4, 5]. In contrast, NLO calculations with the same scale underestimate the π^0 cross section at $\sqrt{s} = 62.4$ GeV. At the same time, it is known that NLO calculations are not always successful at describing low energy fixed target data [9], while NLL calculations have been successful [10]. The

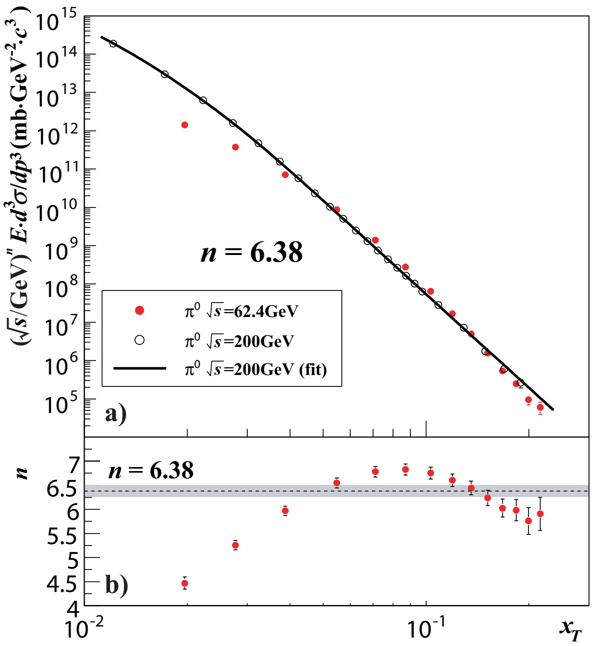

FIG. 4: (color online) (a) The neutral pion production cross section at $\sqrt{s} = 62.4$ GeV and $\sqrt{s} = 200$ GeV as a function of x_T, scaled by $(\sqrt{s}/\mathrm{GeV})^n$ with n=6.38; the solid line is a parameterization of $\sqrt{s} = 200$ GeV data. (b) The parameter n in (6) obtained from the ratio of invariant cross section at $\sqrt{s} = 62.4$ GeV and $\sqrt{s} = 200$ GeV, at each x_T of $\sqrt{s} = 62.4$ GeV data; error bars show the statistical and systematic uncertainties of the $\sqrt{s} = 62.4$ GeV and $\sqrt{s} = 200$ GeV data. The shaded band reflects the 11%⊕9.7% normalization uncertainty in the $\sqrt{s} = 62.4$ and 200 GeV cross section measurements, correspondingly.

NLL calculations have a smaller scale dependence and describe our data well with $\mu = p_T$; however, as noted in [11], subleading perturbative corrections to the NLL calculation may be significant. Therefore, the results may indicate that $\sqrt{s} = 62.4$ GeV is at an intermediate energy region where calculations that include threshold logarithm effects may describe the data more accurately. Therefore, below we show comparisons to both NLO and NLL at a scale of $\mu = p_T$.

General principles of hard scattering, including the principle of factorization of the reaction into parton distribution functions for the protons, fragmentation functions for the scattered partons and a short-distance parton-parton hard scattering cross section, predicted a general x_T-scaling form for the invariant cross section of inclusive particle production near mid-rapidity [26]:

$$E\frac{d^3\sigma}{dp^3} = \frac{1}{p_T^n}F(x_T) = \frac{1}{\sqrt{s}^{\,n}}G(x_T) \qquad (6)$$

where $x_T = 2p_T/\sqrt{s}$, and $F(x_T)$ and $G(x_T)$ are universal functions. The parameter n relates to the form of the force-law between constituents. For example for QED or Vector Gluon exchange, $n = 4$ [27]. Due to higher order effects, the running of the coupling constant $\alpha(Q^2)$, the evolution of the parton distribution functions and fragmentation functions, and the initial-state transverse momentum k_T, n is not a constant but is a function of x_T and $\sqrt{s}$: $n(x_T, \sqrt{s})$ [28].

Figure 4a shows the inclusive π^0 cross section scaled by $\sqrt{s}^{\,n}$ for $\sqrt{s} = 62.4$ GeV and 200 GeV data [5] as a function of x_T, with the parameter $n = 6.38$, which is a weighted average of $n(x_T)$ for $x_T > 0.07$ (corresponding to $p_T > 2$ GeV/c at $\sqrt{s} = 62.4$ GeV). The parameter $n(x_T)$ was calculated as $\ln(\sigma_{62.4}(x_T)/\sigma_{200}(x_T))/\ln(200/62.4)$ for each x_T of $\sqrt{s} = 62.4$ GeV data, and $\sigma_{62.4}$ and σ_{200} are invariant differential cross sections at $\sqrt{s} = 62.4$ GeV and $\sqrt{s} = 200$ GeV, respectively. Cross section values for the corresponding x_T at $\sqrt{s} = 200$ GeV were obtained from parameterization of the measured cross section at $\sqrt{s} = 200$ GeV: $T(p_T)\frac{A}{(1+p_T/p_0)^m} + (1 - T(p_T))\frac{B}{p_T^k}$, $T(p_T) = \frac{1}{1+\exp((p_T-t)/w)}$, where $t = 4.5$ GeV/c, $w = 0.084$ GeV/c, $A = 253.8$ mb·GeV$^{-2} \cdot c^3$, $p_0 = 1.488$ GeV/c, $m = 10.82$, $B = 14.7$ mb·GeV$^{-2+k} \cdot c^{3-k}$, and $k = 8.11$. All $\sqrt{s} = 200$ GeV data points agree with the parameterization curve within uncertainties. The parameterization is shown as the solid curve in Fig. 4a.

At low x_T, where soft physics dominates particle production, $n(x_T)$ is supposed to increase with x_T due to the similar exponential shapes of the soft part of the invariant cross section versus p_T at different $\sqrt{s}$ ($\sim e^{-6p_T}$) [27]. In the hard scattering region $n(x_T)$ is expected to decrease with increasing x_T, due to stronger scale breaking at lower p_T. Such behavior of $n(x_T)$ is demonstrated by our data in Fig. 4b. A similar drop in the parameter n at $x_T \gtrsim 0.1$ was observed at ISR energies [12]. Figure 4b also shows the possible transition from soft- to hard-scattering regions in π^0 production at $p_T \sim 2$ GeV/c. A similar conclusion was derived from the shape of the π^0 spectrum at $\sqrt{s} = 200$ GeV in [5]. This can serve as a basis for applying the pQCD formalism to the double helicity asymmetry data with $p_T > 2$ GeV/c in order to allow access to ΔG.

IV. INCLUSIVE π^0 DOUBLE HELICITY ASYMMETRY

A. π^0 A_{LL} analysis

For the 2006 run, each of the two independent RHIC collider rings were filled with up to 111 bunches in a 120 bunch pattern, with one of four, fill-by-fill alternating predetermined patterns of polarization sign for the bunches. Bunch polarization signs in each pattern were set in such a way that all four colliding bunch spin combinations occurred in sequences of four bunch crossings. That greatly reduced the systematic effects in spin asymmetry measurements due to variation of detector response versus time and due to possible correlation of detector performance with RHIC bunch structure.

To collect data from collisions of longitudinally polarized protons, the polarization orientation of the beams was rotated from vertical, the stable spin direction in RHIC, to longitudinal at the PHENIX IR and then back to vertical after the IR by spin rotators [29]. PHENIX local polarimeters measured the residual transverse component of the beam polarizations, using the spin dependence of very forward neutron production [5, 18, 19] observed by the ZDC, and by that means monitored the orientation of the beam polarization in the PHENIX IR throughout the run.

The magnitudes of the beam polarizations at RHIC are measured using fast carbon target polarimeters [30], normalized to absolute polarization measurements by a separate polarized atomic hydrogen jet polarimeter [31]. The luminosity-weighted beam polarizations over 11 RHIC fills used in the A_{LL} analysis were $\langle P\rangle$=0.48 for both beams, with 0.035 and 0.045 systematic uncertainty for the two RHIC beams, respectively. For the longitudinal polarization run period, the residual transverse polarizations of the beams were $\langle P_T/P\rangle^B$=0.11±0.15 and $\langle P_T/P\rangle^Y = 0.11 \pm 0.12$ for "Blue" and "Yellow" RHIC beams, respectively. The average transverse component of the product was $\langle P_T^B \cdot P_T^Y\rangle/\langle P^B \cdot P^Y\rangle \leq \langle P_T/P\rangle^B \cdot \langle P_T/P\rangle^Y = 0.012 \pm 0.021$; the average of the polarization product over the run was $\langle P^B \cdot P^Y\rangle = 0.23$, with a systematic uncertainty of ±14%.

Experimentally, the double helicity asymmetry for π^0 production is determined as:

$$A_{LL}^{\pi^0} = \frac{1}{|P^B \cdot P^Y|} \cdot \frac{N_{++} - R \cdot N_{+-}}{N_{++} + R \cdot N_{+-}}; \quad R = \frac{L_{++}}{L_{+-}}, \tag{7}$$

where N_{++} and N_{+-} are the number of π^0's and R is the relative luminosity between bunches with the same and opposite helicities. The analysis technique for the π^0 A_{LL} measurements is similar to our analyses of $\sqrt{s} = 200$ GeV data [5, 18, 22].

Double helicity asymmetry results were obtained from longitudinally polarized $p + p$ collisions corresponding to $\sim$ 40 nb^{-1} integrated luminosity. Due to the limited BBC trigger efficiency for high p_T π^0 events, high p_T photon triggered events without the BBC trigger condition requirement were used for the π^0 asymmetry analysis. This led to a slightly increased background in the π^0 reconstruction and additional systematic uncertainty in the measurements of the relative luminosity between bunches with different helicity states.

The background asymmetry under the π^0 peak in the two-photon mass distribution A_{LL}^{BG} was estimated from the counts outside the π^0 peak, from a 177–217 MeV/c^2 range in the two-photon mass distribution. Unlike our $\sqrt{s} = 200$ GeV data analyses, a lower mass range was not used for A_{LL}^{BG} estimations due to cosmic background from non-collision events. This background contribution in the mass ranges of π^0 peak and higher mass was negligible ($< 1\%$), and A_{LL}^{BG} was consistent with zero in all p_T bins.

Similar to our previous analyses, crossing-by-crossing accumulated number of BBC triggers were used for the measurements of the relative luminosity between bunches with different spin configuration. The uncertainty on the relative luminosity measurements δR was derived from the comparison between BBC trigger events and other trigger events, selecting different physics processes in different kinematic ranges. In the $\sqrt{s} = 200$ GeV data analysis the comparison was done to triggers defined by the coincidence of signals from the two ZDCs [5, 18, 22]. Due to the limited efficiency of the ZDC at $\sqrt{s} = 62.4$ GeV, the comparison in this analysis was performed with the number of events which fired simultaneously either of the two BBCs and either of the two ZDCs. Only 20% of the event statistics in this sample is contributed by BBC-triggered events, so this sample can be considered as essentially independent from the BBC event sample. From this comparison the upper limit of δR was estimated to be 0.6×10^{-3}, which for the average beam polarizations of 0.48 translates to $\delta A_{LL} = 1.4\times10^{-3}$, the p_T independent uncertainty of the π^0 double helicity asymmetry results. Single beam background $< 0.35\%$, as determined by the trigger counts of non-colliding bunches and pileup probability of $\lesssim 0.02\%$, had negligible impact on the relative luminosity measurements.

A transverse double spin asymmetry A_{TT}, the transverse equivalent to Eq. (1) and (7), can contribute to A_{LL} through the residual transverse component of the product of the beam polarizations discussed above. Similar to [5], A_{TT} was obtained from the sample with transverse polarization. The maximal possible A_{TT} effect on A_{LL} was determined by $\pm\delta A_{TT}$ from the measured A_{TT}, which was $< 0.15 \cdot \delta A_{LL}$ in all p_T bins.

B. π^0 A_{LL} results and discussion

Figure 5 presents the measured double helicity asymmetry in π^0 production versus p_T [23]. A scale uncertainty of 14% in $A_{LL}^{\pi^0}$ due to the uncertainty in beam polarizations is not shown. The other systematic uncertainties are negligible, as discussed above, and checked using a technique to randomize the sign of bunch polarization and by varying the π^0 identification criteria [18].

Figure 5 also shows a set of A_{LL} curves from pQCD calculations that incorporates different scenarios for gluon polarization within the GRSV parameterization of the polarized parton distribution functions [32]. GRSV-std corresponds to the best fit to inclusive DIS data. The other three scenarios in Fig.5 (GRSV-max, $\Delta G = 0$, and $\Delta G = -G$) are based on the best fit, but use the functions $\Delta G(x_g) = G(x_g), 0, -G(x_g)$ at the initial scale for parton evolution ($Q^2 = 0.4$ GeV^2), where $G(x_g)$ is the unpolarized gluon distribution, and $\Delta G(x_g)$ is the difference between the distribution of gluons with the same and opposite helicity to the parent proton. In Fig. 5, we compare our asymmetry data with both NLO and NLL calculations. The NLL calculations indicate that we have a reduced sensitivity to positive ΔG, but the effect is far less pronounced than at Fermilab fixed-target ener-

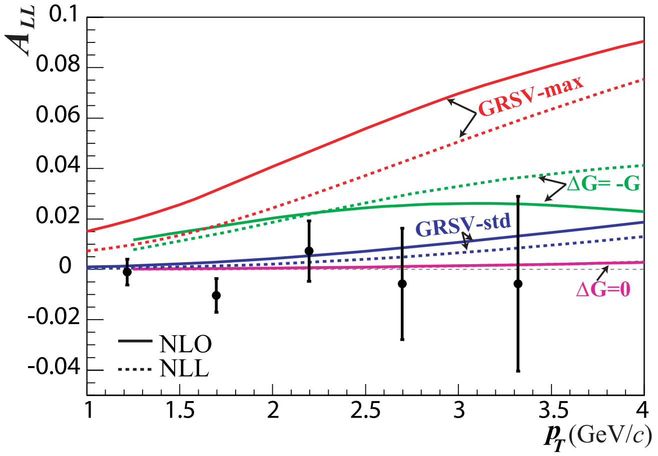

FIG. 5: (color online) The double helicity asymmetry for neutral pion production at $\sqrt{s} = 62.4$ GeV as a function of p_T (GeV/c). Error bars are statistical uncertainties, with the 14% overall polarization uncertainty not shown; other experimental systematic uncertainties are negligible. Four GRSV theoretical calculations based on NLO pQCD (solid curves) and on NLL pQCD (dashed curves) are also shown for comparison with the data (see text for details). Note that the $\Delta G = 0$ curves for NLO and NLL overlap.

gies [11]. Similar to our $\sqrt{s} = 200$ GeV results [5, 18], our $\sqrt{s} = 62.4$ GeV A_{LL} data do not support a large gluon polarization scenario, such as GRSV-max.

Figure 6 presents the measured A_{LL} versus x_T in π^0 production overlaid with the results at $\sqrt{s} = 200$ GeV [5]. Clear statistical improvement can be seen at higher x_T. For the measured p_T range 2–4 GeV/c, the range of x_g in each bin is broad and spans the range $x_g = 0.06 - 0.4$, as calculated by NLO pQCD [33]. Thus our data set extends our x_g reach of sensitivity to ΔG and also overlaps previous measurements, providing measurements with the same x_g but at a different Q^2 scale.

V. SUMMARY

To summarize, we have presented the unpolarized cross section and double helicity asymmetries for π^0 production at mid-rapidity, for proton-proton collisions at $\sqrt{s} = 62.4$ GeV. The accuracy of the cross-section measurements, which fall within the large spread of ISR data, relies on direct π^0 two-photon decay reconstruction, precise calibration of the photon energy measurements, careful study of the trigger performance and accurate control of the integrated luminosity of the analyzed data sample. The results serve as a precise baseline for heavy-ion measurements. Comparisons to NLO and NLL theoretical calculations indicate that including the effects of threshold logarithms may be necessary to more accurately describe the cross section at $\sqrt{s} = 62.4$ GeV. The A_{LL} results extend the sensitivity to the polarized gluon distribution in the proton to higher x_g compared to the previous measurements at $\sqrt{s} = 200$ GeV. A preliminary version of these double helicity asymmetry results was already used in a recent global fit of both RHIC and polarized DIS data to constrain ΔG [34].

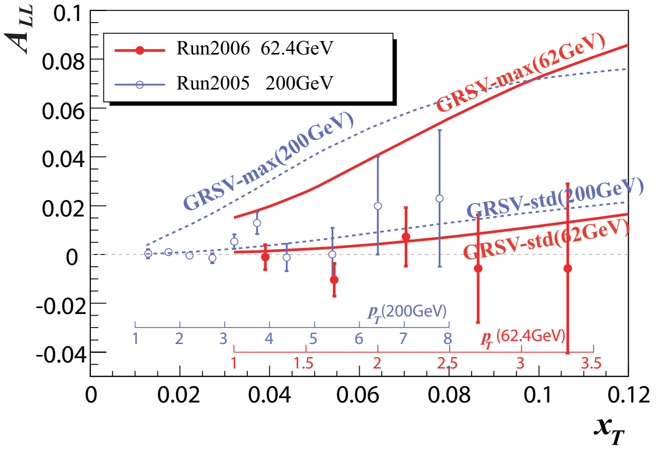

FIG. 6: (color online) The double helicity asymmetry for neutral pion production at $\sqrt{s} = 62.4$ GeV and 200 GeV as a function of x_T. Error bars are statistical uncertainties, with the 14% (9.4%) overall polarization uncertainty for $\sqrt{s} = 62.4$ GeV (200 GeV) data not shown. Two GRSV theoretical calculations based on NLO pQCD are also shown for comparison with the data (see text for details.)

Acknowledgments

We thank the RHIC Polarimeter Group and the staff of the Collider-Accelerator and Physics Departments at Brookhaven National Laboratory and the staff of the other PHENIX participating institutions for their vital contributions. We thank W. Vogelsang and M. Stratmann for providing the pQCD calculations and for informative discussions. We acknowledge support from the Office of Nuclear Physics in the Office of Science of the Department of Energy, the National Science Foundation, a sponsored research grant from Renaissance Technologies LLC, Abilene Christian University Research Council, Research Foundation of SUNY, and Dean of the College of Arts and Sciences, Vanderbilt University (U.S.A), Ministry of Education, Culture, Sports, Science, and Technology and the Japan Society for the Promotion of Science (Japan), Conselho Nacional de Desenvolvimento Científico e Tecnológico and Fundação de Amparo à Pesquisa do Estado de São Paulo (Brazil), Natural Science Foundation of China (People's Republic of China), Ministry of Education, Youth and Sports (Czech Republic), Centre National de la Recherche Scientifique, Commissariat à l'Énergie Atomique, and Institut National de Physique Nucléaire et de Physique des Particules (France), Ministry of Industry, Science and Tekhnologies, Bundesministerium für Bildung und Forschung, Deutscher Akademischer Austausch Dienst, and Alexander von Humboldt Stiftung (Germany), Hungarian National Science Fund, OTKA (Hungary), Department of Atomic Energy (India), Israel Science Foundation (Israel), Korea Research Foundation and Korea Science and Engineering Foundation (Korea), Ministry of Education and Science, Rassia Academy of Sciences, Federal Agency of Atomic Energy (Russia), VR and the Wallenberg Foundation (Sweden), the U.S. Civilian Research and Development Foundation for the Independent States of the Former Soviet Union, the US-Hungarian Fulbight Foundation for Educational Exchange, and the US-Israel Binational Science Foundation.

[1] J. Ashman *et al.* (EMC), Phys. Lett. **B206** 364 (1988), Nucl. Phys. **B328**, 1 (1989).

[2] A. Airapetian *et al.* (HERMES), Phys. Rev. **D75**, 012007 (2007); V.Yu. Alexakhin *et al.* (COMPASS), Phys. Lett. **B647**, 8 (2007).

[3] G. Bunce *et al.*, Ann. Rev. Nucl. Part. Sci. **50**, 525 (2000).

[4] S.S. Adler *et al.* (PHENIX), Phys. Rev. Lett. **91**, 241803 (2003).

[5] A. Adare *et al.* (PHENIX), Phys. Rev. **D76**, 051106 (2007).

[6] J. Adams *et al.* (STAR), Phys. Rev. Lett. **92**, 171801 (2004).

[7] B.I. Abelev *et al.* (STAR), Phys. Rev. Lett. **97**, 252001 (2006).

[8] S.S. Adler *et al.* (PHENIX), Phys. Rev. Lett. **98**, 012002 (2007).

[9] P. Aurenche *et al.*, Eur. Phys. J. **C13**, 347 (2000).

[10] D. de Florian and W. Vogelsang, Phys. Rev. **D71**, 114004 (2005).

[11] D. de Florian, W. Vogelsang, and F. Wagner, Phys. Rev. **D76**, 094021 (2007).

[12] A.L.S. Angelis (CCOR), Phys. Lett. **B79**, 505 (1978); C. Kourkoumelis *et al.* (R-806), Phys. Lett. **B84**, 271 (1979).

[13] A.L.S. Angelis *et al.* (CMOR), Nucl. Phys. **B327**, 541 (1989); T. Akesson *et al.* (AFS), Sov. J. Nucl. Phys. **51**, 836 (1990); C. Kourkoumelis *et al.* (R-806), Z. Phys. **C5**, 95 (1980); A. G. Clark *et al.* (CSZ), Phys. Lett. **B74**, 267 (1978); F. W. Busser *et al.* (CCRS), Nucl. Phys. **B106**, 1 (1976); K. Eggert *et al.* (ACHM), Nucl. Phys. **B98**, 49 (1975); F. W. Busser *et al.* (CCR), Phys. Lett. **B46**, 471 (1973); F. W. Busser *et al.* (CCRS), Phys. Lett. **B55**, 232 (1975); M. Banner *et al.* (Saclay), Nucl. Phys. **B126**, 61 (1977); B. Alper *et al.* (BSC), Nucl. Phys. **B100**, 237 (1975).

[14] D. d'Enterria, J. Phys. **G31**, S491 (2005).

[15] L. Aphecetche *et al.*, Nucl. Instrum. Methods **A499**, 521 (2003).

[16] M. Allen *et al.*, Nucl. Instrum. Methods **A499**, 549 (2003).

[17] C. Adler *et al.*, Nucl. Instrum. Methods **A470**, 488 (2001).

[18] S.S. Adler *et al.* (PHENIX), Phys. Rev. Lett. **93**, 202002 (2004).

[19] Y. Fukao *et al.*, Phys. Lett. **B650**, 325 (2007).

[20] S. van der Meer, ISR-PO/68-31, KEK68-64; A. Drees and Z. Xu, PAC-2001-RPAH116 *Presented at IEEE Particle Accelerator Conference (PAC2001), Chicago, Illinois, 18-22 Jun 2001.*

[21] P. Cameron et al, Proc. of the Particle Accelerator Conference, p.2146 (1999).

[22] S.S. Adler *et al.* (PHENIX), Phys. Rev. **D73**, 091102 (2006).

[23] Tables of data available at http://www.phenix.bnl.gov /phenix/WWW/info/data/ppg087_data.html

[24] A. D. Martin *et al.*, Eur. Phys. J. C **35**, 325 (2004)

[25] D. de Florian *et al.*, Phys. Rev. **D75**, 114010 (2007).

[26] R. Blankenbecler, S.J. Brodsky and J.F Gunion, Phys. Lett. **B42**, 461 (1972).

[27] S.M. Berman, J.D. Bjorken and J.B Kogut, Phys. Rev. **D4**, 3388 (1971).

[28] R. F. Cahalan, K. A. Geer, J. B. Kogut, and L. Susskind, Phys. Rev. **D11**, 1199 (1975).

[29] W.W. MacKay *et al.*, Proceedings of the 2003 Particle Accelerator Conference, edited by J. Chew, P. Lucas and S. Webber, IEEE, p.1697.

[30] O. Jinnouchi *et al.*, RHIC/CAD Accelerator Physics Note 171 (2004).

[31] H. Okada *et al.*, Phys. Lett. **B638**, 450 (2006).

[32] B. Jäger *et al.*, Phys. Rev. **D67**, 054005 (2003); M. Glück *et al.*, Phys. Rev. **D63**, 094005 (2001).

[33] M. Stratmann and W. Vogelsang, hep-ph/0702083 = J. Phys. Conf. Ser. **69**, 012035 (2007); W. Vogelsang, private communication.

[34] D. de Florian *et al.*, Phys. Rev. Lett. **101**, 072001 (2008).

[35] D.L. Adams *et al.*, Phys. Lett. B **261**, 197 (1991).